Since January 2020 Elsevier has created a COVID-19 resource centre with free information in English and Mandarin on the novel coronavirus COVID-19. The COVID-19 resource centre is hosted on Elsevier Connect, the company's public news and information website.

Elsevier hereby grants permission to make all its COVID-19-related research that is available on the COVID-19 resource centre - including this research content - immediately available in PubMed Central and other publicly funded repositories, such as the WHO COVID database with rights for unrestricted research re-use and analyses in any form or by any means with acknowledgement of the original source. These permissions are granted for free by Elsevier for as long as the COVID-19 resource centre remains active.

Phytomedicine 95 (2022) 153874

Contents lists available at ScienceDirect

Phytomedicine

journal homepage: www.elsevier.com/locate/phymed

Effect of Jinzhen granule on two coronaviruses: The novel SARS-CoV-2 and the HCoV-229E and the evidences for their mechanisms of action

Qinhai Ma [a,#], Zhoulang Wang [a,#], Ruihan Chen [a,#], Biao Lei [a], Bin Liu [a], Haiming Jiang [a], Zexing Chen [a], Xuejun Cai [a], Xiaowen Guo [a], Meihua Zhou [a], Jicheng Huang [c,*], Xiaobo Li [c,*], Jun Dai [c,*], Zifeng Yang [a,b,*]

[a] State Key Laboratory of Respiratory Disease, National Clinical Research Center for Respiratory Disease, Guangzhou Institute of Respiratory Health, the First Affiliated Hospital of Guangzhou Medical University, Guangzhou, Guangdong, postcode, PR China
[b] Guangzhou Laboratory, Guangdong, postcode, PR China
[c] Technology Centre, Guangzhou Customs, Guangzhou, PR China

ARTICLE INFO

Keywords:
Jinzhen granule
Coronaviruses
SARS-CoV-2
HCoV-229E
Antiviral
Anti-inflammatory

ABSTRACT

Background: Although severe acute respiratory syndrome coronavirus 2 (SARS-CoV-2) and human coronavirus 229E (HCoV-229E) pose a huge threat to human public health, no specific treatment is available. Jinzhen granule (JZ) is a traditional eight ingredients-Chinese medicine with prominent efficacy for treating viral-induced diseases. However, little is known about the antiviral effect and mechanism of JZ against SARS-CoV-2 and HCoV-229E.

Purpose: This study aimed to reveal the antiviral effects of JZ against SARS-CoV-2 and HCoV-229E, and to further explore the underlying mechanisms regulating the host immune response.

Methods: The chromatographic separation of JZ was performed using a Shimadzu analytical high-performance liquid chromatograph with UV detection and Alltech ELSD 2000ES. We conducted cytopathic effect (CPE) and plaque reduction assays to evaluate the antiviral effect of JZ. A lethal human angiotensin converting enzyme 2 (hACE2) transgenic mouse model of SARS-CoV-2 was established to determine the protective effect of JZ on mortality and lung virus titers. Real-time quantitative PCR assays were used to analyze the expression of proinflammatory cytokines *in vitro* and *in vivo*. Western blotting was further performed to determine the activities on regulating the nuclear factor kappa B (NF-κB)/MAPK pathway. Finally, mitochondrial membrane potential assays, flow cytometry analysis and western blotting were used to assess the anti-apoptotic potency toward HCoV-229E infection.

Results: The results showed that 13 chemical components were identified and five peaks were determined and quantitated (gallic acid 1.97 mg/g, baicalin 20.69 mg/g, glycyrrhizic acid 4.92 mg/g, hyodeoxycholic acid 4.86 mg/g, cholic acid 4.07 mg/g). We found that JZ exerted inhibitory potency against SARS-CoV-2 and HCoV-229E *in vitro* by using CPE and plaque reduction assays, and it was further found that JZ protected mice infected by SARS-CoV-2 from death and inhibited lung virus titers. JZ also significantly decreased the induction of inflammatory cytokines (IL-1α, IL-6, CCL-5 and MIP-1β), similar to the observed in vitro effect. Moreover, JZ suppressed the release of inflammatory cytokines in vitro and it decreased the protein expression of p-p38 MAPK,

Abbreviations: CC_{50}, 50% cytotoxicity concentration; CCCP, carbonyl cyanide m-chlorophenylhydrazone; COVID-19, coronavirus disease 2019; CPE, Cytopathic effect; cytC, cytochrome c; DMEM, Dulbecco's modified Eagle's medium; DMSO, Dimethyl sulfoxide; EC_{50}, half maximal effective concentration; FBS, fetal bovine serum; GAPDH, Glyceraldehyde 3-phosphate dehydrogenase; G-CSF, Granulocyte colony-stimulating factor; HCoV-229E, human coronavirus 229E; Huh-7, hepatocellular carcinoma cell line; IC_{50}, 50% inhibition concentrations; IL-1β, Interleukin-1beta; IL-6, Interleukin-6; IP-10, Interferon-inducible protein-10; JZ, Jinzhen granule; MAPK, mitogen activated protein kinase; MCP-1, Monocyte chemoattracctant protein-1; MERS-CoV, Middle East respiratory syndrome coronavirus; MIP-1a, Recombinant Macrophage Inflammatory Protein 1 alpha; MOI, multiplicity of infection; NF-κB, nuclear transcription factor-kappa B; NHP, nonhuman primates animal model; PARP, poly (ADP-ribose) polymerase; PBS, Phosphate-buffered saline; PFU, plaque forming-unit; RT-qPCR, Real-time Fluorescent Quantitative Polymerase Chain Reaction; SARS-CoV, severe acute respiratory syndrome coronavirus; SI, selective index; $TCID_{50}$, 50% tissue culture infective dose; TCM, Traditional Chinese medicine; TNF-α, Tumor necrosis factor-α; Vero E6, African green monkey kidney epithelial cell line; VGM, virus growth medium.

* Corresponding authors.
E-mail addresses: huangjc@iqtc.cn (J. Huang), lixb@iqtc.cn (X. Li), daij@iqtc.cn (J. Dai), jeffyah@163.com (Z. Yang).
# Qinhai Ma, Zhoulang Wang and Ruihan Chen have equal contributions to this study.

https://doi.org/10.1016/j.phymed.2021.153874
Received 30 June 2021; Received in revised form 23 November 2021; Accepted 29 November 2021
Available online 11 December 2021
0944-7113/© 2021 Elsevier GmbH. All rights reserved.

p-JNK, p-NF-κB p65 and p-IκBα induced by HCoV-229E and increased the expression of IκBα. Notably, JZ significantly protected HCoV-229E-infected Huh-7 cells from mitochondrial damage and decreased apoptotic cells. The activation of the mitochondria-mediated apoptotic pathway was inhibited by JZ, as shown by the reduced expression of cleaved caspase-9, caspase-3 and p-PARP.

Conclusions: In conclusion, JZ (gallic acid 1.97 mg/g, baicalin 20.69 mg/g, glycyrrhizic acid 4.92 mg/g, hyodeoxycholic acid 4.86 mg/g, cholic acid 4.07 mg/g) exhibited antiviral activities against SARS-CoV-2 and HCoV-229E by regulating the NF-κB/MAPK pathway and the mitochondria-mediated apoptotic pathway. These findings demonstrated the efficacy of JZ against CoVs and suggested JZ treatment as a novel clinical therapeutic strategy for COVID-19.

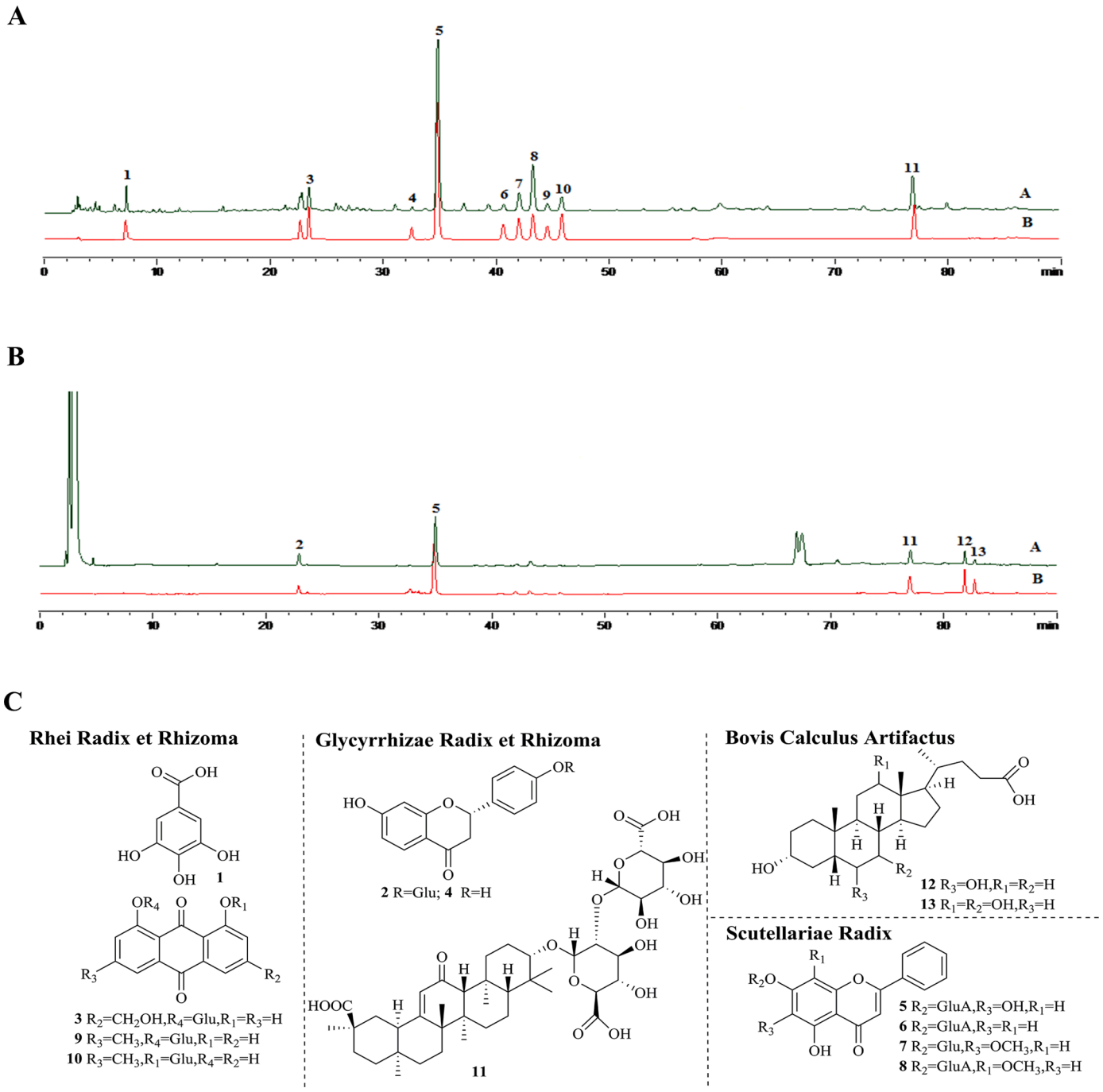

Fig. 1. The chromatographic separation of samples was performed using Shimazu analytical high performance liquid chromatograph with UV detection at 254 nm and Alltech ELSD 2000ES. (A) The HPLC profile of JZ. (B) The HPLC profile of the reference solution. (C) The chemical structures of identified 13 constituents. 1-gallic acid; 2-liquiritin; 3-aloe-emodin-8-O-β-D-glucopyranoside; 4-liquiritigenin; 5-baicalin; 6-chrysin-7-O-β-D-glucoronide; 7-oroxyloside; 8-wogonoside; 9-chrysophal-8-O-β-D-glucopyranoside; 10-chrysophal-1-O-β-D-glucopyranoside; 11-glycyrrhizic acid; 12-hyodeoxycholic acid; 13-cholic acid.

Introduction

Coronaviruses are enveloped, single-stranded, positive-stranded RNA viruses that infect vertebrates including humans. Coronavirus belongs to of the family Coronaviridae, which comprises the sub-families Coronavirinae and Torovirinae (Fehr and Perlman, 2015). There are six known Coronavirinae that can infect humans thus far, including human coronavirus 229E (HCoV-229E), OC43 (HCoV-OC43), NL63 (HCoV-NL63), HKU1 (HCoV-HKU1), severe acute respiratory syndrome coronavirus (SARS-CoV) and Middle East respiratory syndrome coronavirus (MERS-CoV) (Su et al., 2016). Infection by HCoV-229E, HCoV-OC43, HCoV-NL63 and HCoV-HKU1 in healthy adults mostly results in the common cold with clinical symptoms that include fever, cough, sneezing and headache, while infections with these viruses can also be severe in infants, elderly people, and immunocompromised patients (Gorse et al., 2009). They were not regarded as highly pathogenic to humans until SARS-CoV emerged in 2002 and 2003 in Guangdong Province of China. Additionally, another outbreak of the highly pathogenic coronavirus MERS-CoV emerged in 2012 in Middle Eastern countries. From December 2019, a novel coronavirus (SARS-CoV-2) associated with severe respiratory illness and human-to-human transmission has been reported around the world (Wang et al., 2020).

SARS-CoV-2 causes life-threatening respiratory disease similar to the other two highly pathogenic coronaviruses SARS-CoV and MERS-CoV. There were 94.4% identical amino acid sequences used in the classification of coronavirus species between SARS-CoV-2 and SARS-CoV, suggesting that the two coronaviruses seem to be part of the same species, SARS-CoV, although SARS-CoV-2 seems to exhibit more rapid human-to-human transmission (Chen et al., 2020b). In addition, individuals susceptible to SARS-CoV-2 resulted in massive outbreaks that rapidly evolved into public health events, thus generating the declaration of a Public Health Emergency of International Concern (PHEIC) by the World Health Organization (WHO, 2020). The respiratory illness caused by SARS-CoV-2 is associated with intensive care unit (ICU) admission and high mortality (Huang et al., 2020). In response to this pandemic, global researchers have undertaken the unprecedented development of safe treatments and vaccines. A considerable number of SARS-CoV-2 vaccine projects were launched soon after the first description of this virus. To date, many vaccines have already been approved by regulatory authorities in certain countries (Wang et al., 2021a). Nevertheless, there still exists a number of scientific unknowns regarding the effectiveness and safety of COVID-19 vaccines, especially SARS-CoV-2, which already has several variants. Additionally, effective specific antiviral treatment for infection caused by SARS-CoV-2 remains unavailable thus far. Although compounds against SARS-CoV-2 in vitro replication have been reported, the efficacy and safety of drugs for SARS-CoV-2 infection patients remain to be further assessed (Lu, 2020). Thus, there exists an urgent need to identify an effective agent for treating SARS-CoV-2 infection.

Traditional Chinese medicine (TCM) has played a crucial role in the prevention and treatment of COVID-19, especially in mild cases (Ma et al., 2020; Nile and Kai, 2020; Wang et al., 2021b). Jinzhen granule (JZ), a TCM formula approved by the China Food and Drug Administration (CFDA), comprises eight ingredients. Of them, four are medicinal plants: the bulb of Fritillaria ussuriensis Maxim. (Liliaceae) (Fritillariae Ussuriensis Bulbus); root and rhizome of Rheum palmatum l. (Polygonaceae) (Rhei Radix et Rhizoma); root of Scutellaria baicalensis Georgi (Lamiaceae) (Scutellariae Radix) and root and rhizome of Glycyrrhiza uralensis Fisch. (Fabaceae) (Glycyrrhizae Radix et Rhizoma); two are of animal origin (Bovis Calculus Artifactus and Caprae Hircus Cornu) and two are of mineral origin (Chloriti Lapis and Gypsum Fibrosum). JZ has become a frontline medicine in China used to treat some viral infections in hands, feet and mouth (HFMD) of children (Liu et al., 2014). Besides, JZ could suppress the replication of influenza, respiratory syncytial virus (RSV) and SARS *in vitro* (Hou et al., 2009). It has been reported that the potential antiviral and anti-inflammatory mechanism of JZ is associated with inhibiting protein phosphorylation levels and blocking the nuclear transcription factor-kappa B (NF-κB) and mitogen activated protein kinase (MAPK) inflammatory pathways (Zong et al., 2018). Unfortunately, there exists insufficient evidence to support its broad-spectrum pharmacological properties in treating coronavirus. Consequently, we assessed the antiviral and anti-inflammatory activities of JZ against clinically isolated SARS-CoV-2 and HCoV-229E in vitro and in vivo in order to be able to suggest JZ as a potential agent for clinical use in the treatment of SARS-CoV-2. Moreover, our results from this study can help to clarify the underlying mechanism of JZ against SARS-CoV-2 and HCoV-229E infection.

Materials and methods

Reagents

JZ (lot: 130,110) used in this study was produced and provided by Kanion Pharmaceutical Co., Ltd. (Jiangsu, China). Gallic acid (110,831–201,605), liquiritin (111,610–201,607), baicalin (110,715–201,720), wogonoside (112,002–201,702), hyodeoxycholic acid (100,087–201,411), and cholic acid (100,078- 201,415) were purchased from China Food and Drug Testing Institute (Beijing, China). Chrysin-7-O-β-D-glucuronide (PRF10080201), oroxyloside (PRF10081603), and chrysophanol-1-O-β-D-glucopyranoside (PRF10040201) were obtained from Chengdu Mansite reference material Co., Ltd (Chengdu, China). Chrysophanol-8-O-β-D-glucopyranoside (P19J9S66043), glycyrrhizic acid (P24J10F91300), aloe-emodin-8-O-β-D-glucopyranoside (X20J9×66,041) were obtained from Yuan Ye Biological Co., Ltd (Shanghai, China). liquiritigenin (DST190920–010) were purchased from Durst Biological Co. Ltd. (Chendu, China). The chromatographic separation of JZ was performed using a Shimadzu analytical high-performance liquid chromatograph (Kyoto, Japan) with UV detection at 254 nm and Alltech ELSD 2000ES. The separation was developed on KromasiL C18 (4.6 mm × 150 mm, 5 μm) by gradient elution with methanol (B) and water (0.1% formic acid in water, v/v) held at 35 ℃, with a flow rate of 1.0 ml/min. The temperature of the ELSD drift tube was maintained at 115 ℃, and the carrier gas flow rate was 2.0 l/min. The following linear elution gradient program was used: 0–9 min, 8–40% B; 9–30 min, 40%−62% B; 30–40 min, 62%−70% B, 40–54 min, 70–100%. The HPLC-UVD-ELSD fingerprint of JZ was established with good separation, and 13 chemical components were identified (Fig. 1). Five peaks (gallic acid; baicalin; glycyrrhizic acid; hyodeoxycholic acid; and cholic acid) were determined simultaneously, and the contents of 5 components in JZ were quantitated (gallic acid 1.97 mg/g, baicalin 20.69 mg/g, glycyrrhizic acid 4.92 mg/g, hyodeoxycholic acid 4.86 mg/g, cholic acid 4.07 mg/g). Remdesivir (GS-5734) was provided by Gilead Sciences Inc. (Foster, CA, USA) and served as a positive drug control. GAPDH (lot: 2118), p38 (lot: 8690), p-p38 (lot: 4631), IκBα (lot: 4812), p- IκBα (lot: 2859), SAPK/JNK (lot: 9252), p-SAPK/JNK (lot: 4668), Caspase-3 (lot: 9662), Cleaved-Caspase-3 (lot: 9664), PARP (lot: 9532) and p-PARP (lot: 5625) were purchased from Cell Signaling Technology, Inc. (Danvers, MA, USA). Caspase-9 (lot: ab32539) and Cleaved-Caspase-9 (lot: ab2324) were provided by Abcam, Inc. (Cambridge, UK). All the above antibodies were rabbit polyclonal antibodies.

Virus and cells

African green monkey kidney epithelial (Vero E6) cells and human hepatocellular carcinoma cell lines (Huh-7) were cultured in Dulbecco's modified Eagle's medium (DMEM, Gibco, Grand Island, NY, USA) supplemented with 10% fetal bovine serum (FBS, ExCell Biotech, Shanghai, China), and the antibiotics 100 U/ml penicillin, 100 μg/ml streptomycin (Gibco). Cells were maintained at 37 ℃ under a 5% CO_2 atmosphere. SARS-CoV-2 (Genebank accession no. MT123290.1) was a clinical isolate from the First Affiliated Hospital of Guangzhou Medical

Table 1
Primer sequence for RT-qPCR.

Target Gene	Direction	Sequence (5′−3′)
TNF-α (human)	Forward	AACATCCAACCTTCCCAAACG
	Reverse	GACCCTAAGCCCCCAATTCTC
IL-1α (human)	Forward	GAAGATGTGCCTGTCCTGTGT
	Reverse	CGCTCAGGTCAGTGATGTTAA
IL-6 (human)	Forward	CGGGAACGAAAGAGAAGCTCTA
	Reverse	CGCTTGTGGAGAAGGAGTTCA
CCL-5 (human)	Forward	CAGCAGTCGTCTTTGTCACC
	Reverse	GTTGATGTACTCCCGAACCC
MIP-1β (human)	Forward	AAAACCTCTTTGCCACCAATACC
	Reverse	GAGAGCAGAAGGCAGCTACTAG
IL-8 (human)	Forward	CTTGGTTTCTCCTTTATTTCTA
	Reverse	GCACAAATATTTGATGCTTAA
MCP-1 (human)	Forward	CAAGCAGAAGTGGGTTCAGGAT
	Reverse	AGTGAGTGTTCAAGTCTTCGGAGTT
IL-1α (mouse)	Forward	CAGGATGTGGACAAACACTATCT
	Reverse	CTCACGAACAGTTGTGAATCTGA
IL-6 (mouse)	Forward	ACAAGAAAGACAAAGCCAGAGTCC
	Reverse	CTGTTAGGAGAGCATTGGAAATTG
CCL-5 (mouse)	Forward	CTTGAACCCACTTCTTCTCTGG
	Reverse	TGCTGCTTTGCCTACCTCTC
MIP-1β (mouse)	Forward	TTCTGTGCTCCAGGGTTCTC
	Reverse	CGGGAGGTGTAAGAGAAACAG
GAPDH (human)	Forward	GAAGGTGAAGGTCGGAGTC
	Reverse	GAAGATGGTGATGGGATTTC
GAPDH (mouse)	Forward	CAAAATGGTGAAGGTCGGTGTG
	Reverse	GTTGAGGTCAATGAAGGGGTCG

University, propagated and adapted as previously described (Zhu et al., 2019). HCoV-229E (ATCC®VR740™) was purchased from ATCC (American type culture collection) (Manassas, VA, USA) and propagated in Huh-7 cells to create working stocks. The 50% tissue culture infective dose ($TCID_{50}$) of SARS-CoV-2 ($TCID_{50} = 10^{-6.5}$/100 μl) and HCoV-229E ($TCID_{50} = 10^{-6}$/100 μl) was determined by using the Reed-Muench method on Vero E6 and Huh-7 cells, respectively. Virus working stocks were collected and stored at −80 ℃. All SARS-CoV-2 infection experiments were performed in a biosafety level-3 (BLS-3) laboratory.

Cytotoxicity and cytopathic effect (CPE) inhibition assays

The 50% toxicity concentrations (TC_{50}) of JZ and remdesivir against Huh-7 and Vero E6 cells were determined using the MTT assay (Park et al., 2011). Different dilutions of JZ and remdesivir were incubated with Vero E6 (5×10^4 cells/well) and Huh-7 (5×10^4 cells/well) cells in 96-well plates for the cytotoxicity assay, and the TC_{50} values of JZ and remdesivir were calculated.

The 50% inhibition concentration (IC_{50}) of virus-induced CPE was used to investigate the efficacy of JZ and remdesivir against SARS-CoV-2. Briefly, a monolayer of Vero E6 cells was inoculated with 100 $TCID_{50}$ of virus at 37 ℃ for 2 h, and the cells were incubated with different concentrations of JZ and remdesivir after the removal of the inoculum. Infected cells were observed under a microscope after 72 h of incubation. The IC_{50} value was calculated, and the selectivity index (SI) was determined based on the ratio of TC_{50} to IC_{50} (Reed and Muench, 1938).

Plaque reduction assay

Vero E6 and Huh-7 cells were plated in 12-well plates and incubated at 37 ℃ and 5% CO_2 with saturated humidity overnight to form a monolayer. Cells were washed twice with phosphate-buffered saline (PBS) and then infected with SARS-CoV-2 and HCoV-229E for 2 h, respectively. After that, virus-containing media were aspirated and the cell monolayer was overlaid by a 1.5 ml agarose/basic medium mixture containing 0.8% low-melt agarose and the indicated concentration of JZ. Plates were incubated at 37 ℃ and 5% CO_2 with saturated humidity for 72 h. Following incubation, the cell monolayer was fixed with 4% paraformaldehyde for 30 min and stained with 0.1% crystal violet for 5 min to visualize the plaque and counted as previously described (Reed and Muench, 1938).

RNA isolation and reverse transcriptase-quantitative PCR analysis (RT-qPCR)

Huh-7 cells grown in 6-well plates were rinsed with PBS and then infected with SARS-CoV-2 and HCoV-229E at a multiplicity of infection (MOI) of 1 PFU/cell and 0.1 PFU/cell for 2 h, respectively. Afterward, the inocula were removed and the cells were separated into the following six groups: no-treatment control group (NC), virus-infected group (virus), and three groups consisting of nontoxic concentrations of JZ and remdesivir. The cells were harvested at 48 h post-infection. Total RNA of different groups was extracted in accordance by using Trizol reagent (Invitrogen, Carlsbad, MA, USA), and reverse transcription of RNAs was quantified by using the PrimeScript™ RT Master Mix kit (Takara Bio, Tokyo, Japan). Moreover, RT-qPCR was performed on cDNA samples by using SYBR Premix Ex Tap™ II (Takara Bio) and PCR data were analyzed with an ABI PRISM®7500 Real-time PCR detection system (Applied Biosystems Co., Foster, CA, USA). The relative quantity of PCR products was calculated using the $2^{-\Delta\Delta Ct}$ method as previously described (Pfaffl, 2001). The primers of TNF-α, IL-1α, IL-6, CCL-5, MIP-1β, IL-8, MCP-1 and GAPDH were designed using primer 5.0 (Table 1).

Western blotting assay

Cells were treated as described in the "RNA isolation and Fluorescent Quantitative Polymerase Chain Reaction (RT-qPCR) assay" section and harvested for western blot analysis. Cells were lysed on ice for 30 min in radioimmunoprecipitation assay (RIPA) buffer (DGCS Biotechnology, Beijing, China) containing 0.5 mM PMSF, 100 μM β-glycerol 3-phosphate and 0.5% protease inhibitor cocktail. The cell lysate was then cleared by centrifugation at 12,000 × g for 15 min and the supernatant protein contents were determined by using the BCA kit (Beyotime, Shanghai, China). Equal amounts of proteins (20 μg) were size fractionated by 10% sodium dodecyl sulfate polyacrylamide gel electrophoresis (SDS-PAGE) and transferred onto polyvinylidene fluoride (PVDF) membranes (Millipore, Burlington, MA, USA). After blocking with 5% BSA in TBS containing 0.1% Tween 20 for 1 h, the membranes were incubated overnight with the desired primary antibodies at 4 °C. The membranes were then probed with the appropriate HRP-conjugated secondary antibody for 1 h at room temperature, and the immunoreactive bands were visualized using enhanced chemiluminescence (ECL) reagents (FDbio, Hangzhou, China).

Determination of apoptosis levels by flow cytometry

Apoptosis was determined using an Annexin V-FITC apoptosis detection kit according to the manufacturer's protocol (Vazyme Biotech Co., Ltd, Nanjing, China) by staining cells with Annexin V-FITC and propidium iodide (PI). Huh-7 cells grown in 6-well plates were infected with HCoV-229E at 0.1 MOI for 2 h. The inocula were discarded, and cells were subsequently incubated in VGM containing different indicated concentrations of JZ for 48 h. After digestion, cells were harvested by centrifugation at 1000 × g for 5 min and washed twice with PBS. Cells were re-suspended in 100 ml of loading binding buffer and stained with 5 ml of Annexin V-FITC and 5 ml of PI for 15 min at room temperature in the dark. The fluorescent signal of the cells was measured with a flow cytometer (BD Biosciences, San Jose, CA, USA) according to the procedure described previously (Zhang et al., 2010).

Mitochondrial membrane potential assay

Mitochondrial transmembrane potential (ΔΨm) was measured with a mitochondrial membrane potential assay kit with JC-1 (Beyotime).

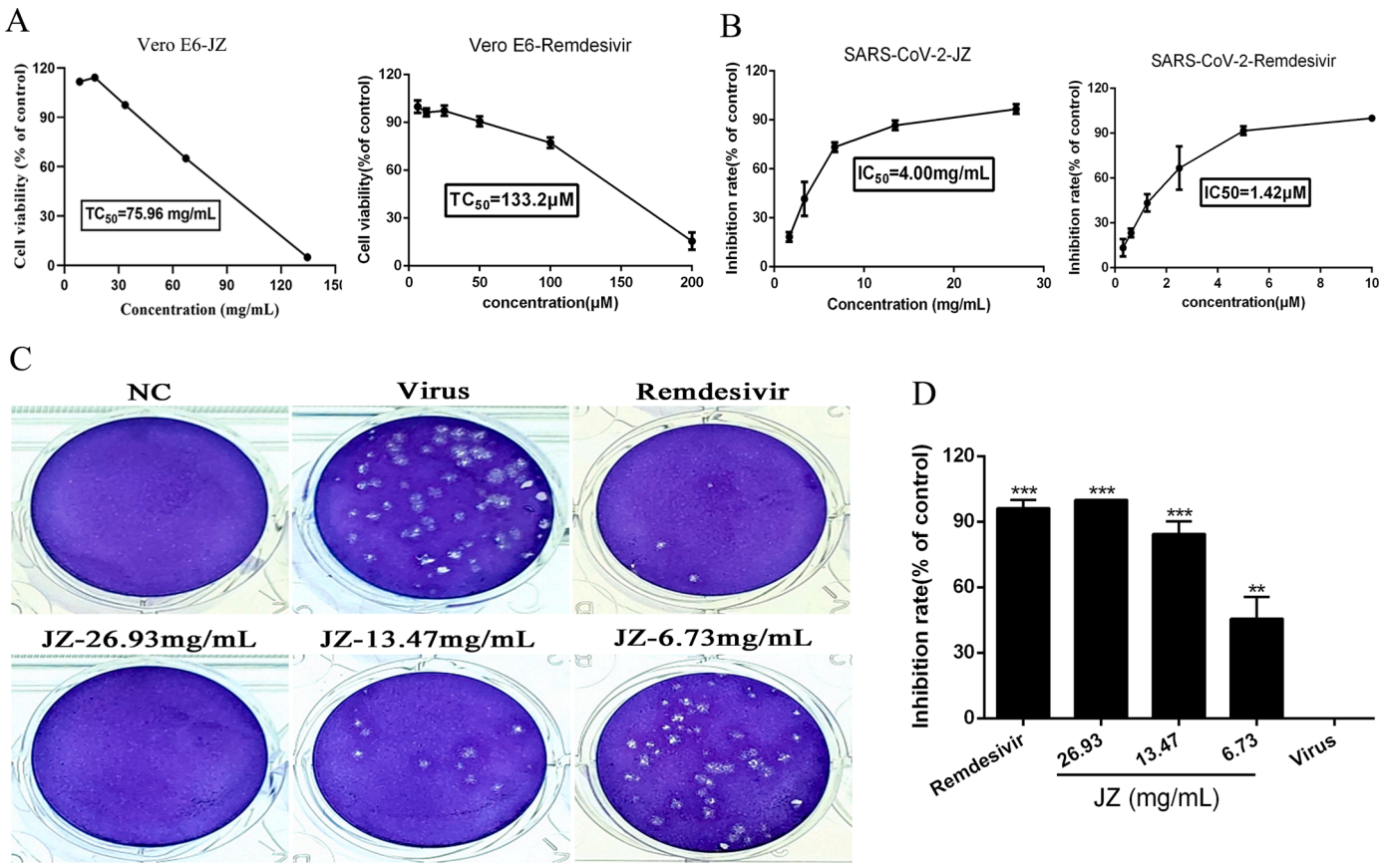

Fig. 2. The inhibition effects of JZ on SARS-CoV-2 in vitro. (A) The cytotoxicity effects of JZ and remdesivir in Vero E6 cells was detected using a MTT assay. (B) The inhibitory effects of JZ and remdesivir on SARS-CoV-2 *in vitro*. (C) Inhibitory effect of JZ and remdesivir on plaque formation of SARS-CoV-2. (D) The quantitative analysis of the plaque formation in different groups was analyzed by SPSS ver. 25.0. Data were presented as the mean ± SD obtained from three separate experiments. * $p < 0.05$; ** $p < 0.01$; *** $p < 0.001$, compared with SARS-CoV-2-infected cells.

Cells were infected with HCoV-229E at 0.1 MOI for 2 h in 12-well plates. After 2 h of incubation, cells were incubated in VGM containing three indicated concentrations of JZ for 48 h. Cells were then incubated at 37 °C for 20 min with 0.5 ml of JC-1 working solution. After that, the staining solution was removed, and the cells were washed twice with JC-1 staining 1× buffer. Finally, ΔΨm was observed by fluorescence microscopy at 100 × (Leica Micro-systems CMS GmbH inverted fluorescence microscope). Red emission of the dye represented a potential-dependent aggregation in the mitochondria, reflecting ΔΨm. Green fluorescence represented the monomeric form of JC-1, appearing in the cytosol after mitochondrial membrane depolarization. Cells treated with 10 μM carbonyl cyanide m-chlorophenylhydrazone (CCCP) were used as a negative control. CCCP is a protonophore that can cause dissipation of ΔΨm.

Antiviral and anti-inflammatory activity of JZ in vivo

This animal study was approved by the Guangzhou Medical University Ethics Committee of Animal Experiments. All animal experiments passed the ethical review and were performed in strict accordance with the National Research Council Criteria and the Chinese Animal Protection Act (GZL0008). Five-to six-week-old female ACE2 transgenic C57BL/6 mice weighing 18–22 g were acquired from GemPharmatech Co., Ltd. (Jiangsu, China) and housed under specific pathogen-free (SPF) conditions at Guangzhou Customs District, P.R. China. Mice were randomly divided into six groups of five mice per group: the control group (non-infected), SARS-CoV-2 virus infected group, remdesivir (50 mg/kg/day) treatment group and three different concentrations (224 mg/kg/day, 448 mg/kg/day, 896 mg/kg/day) of JZ treatment groups.

To determine the antiviral and anti-inflammatory effects of JZ *in vivo*, mice were anesthetized by inhalation of 5% isoflurane and inoculated with 50 μl of 10^5 PFU SARS-CoV-2 in the infected groups and PBS in the control group intranasally. The infected mice were intragastrically administered with JZ (896 mg/kg/day, 448 mg/kg/day or 224 mg/kg/day for 5 days), remdesivir (50 mg/kg/day for 5 days) or PBS 24 h prior to viral infection. After administration, the mice were sacrificed and the lung tissues were harvested to test virus titers. Furthermore, the expression of lung inflammatory cytokines and chemokines was detected by RT-qPCR. To obtain the protective effects of JZ on mice against the SARS-CoV-2, the infected mice were intranasally inoculated with 50 μl of viral suspension consisting of 10^5 PFU SARS-CoV-2. After oral administration for 5 days, the mortality of mice in various groups was observed daily for 5 days to evaluate the protective effects of JZ based on the mice survival time and mortality reduction.

Statistical analysis

All data in this study were analyzed by using analysis of variance (ANOVA) with SPSS ver. 25.0 (Armonk, NY, USA) (Cavic et al., 2021; Jan et al., 2021). The results were expressed as the mean ± standard deviation. Statistical differences in multiple groups were evaluated by one-way ANOVA with Tukey's honest significant difference test. A p value < 0.05 was considered as statistically significant.

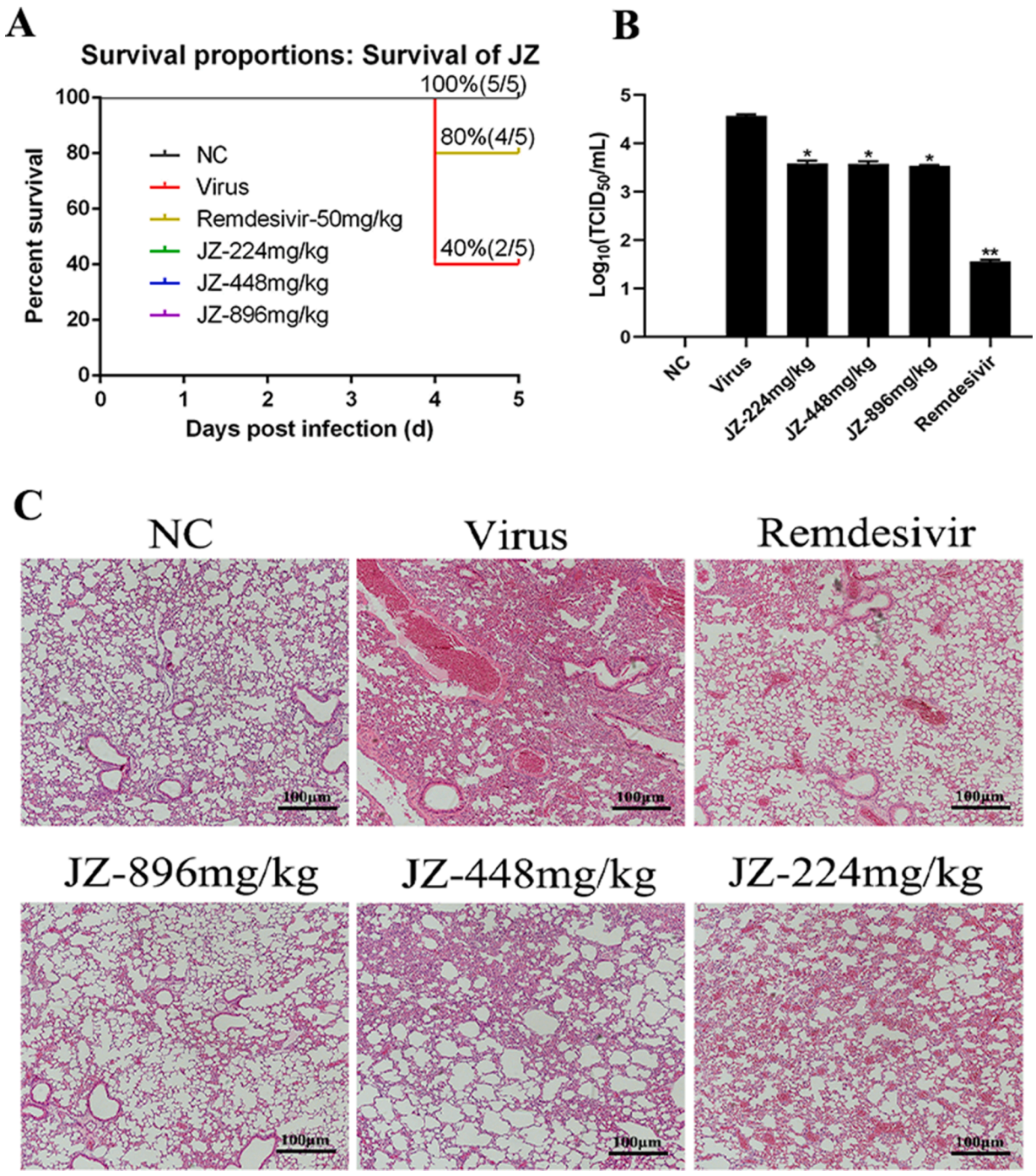

Fig. 3. The protective effects of JZ against SARS-CoV-2 in mouse model. (A) The survival of mice was monitored daily for 5 days after viral infection, and the survival rate was calculated. (B) Virus titers for mice at the fifth d.p.i. (C) Histological observations of lung tissues for mice sacrificed at the fifth d.p.i. Scale bar = 100 μm. * $p < 0.05$; ** $p < 0.01$, *** $p < 0.001$, when compared to the viral control.

Results

The inhibition effects of JZ on SARS-CoV-2 in vitro

The cytotoxicity of JZ and remdesivir in Vero E6 cells was evaluated by a non-radioactive cell proliferation assay (MTT). The TC_{50} values for JZ and remdesivir in Vero E6 cells were 75.96 mg/ml and 133.2 μM, respectively. The antiviral activities of JZ against SARS-CoV-2 were evaluated using CPE inhibition assay and plaque reduction assay (Fig. 2). JZ (26.93 mg/ml, 13.47 mg/ml and 6.73 mg/ml) significantly reduced the CPE caused by infection in Vero E6 cells, the IC_{50} values of JZ and remdesivir were 4.00 mg/ml and 1.42 μM, and the selectivity index (SI) of JZ and remdesivir were 19.00 and 94.00, respectively. A plaque-reduction assay was conducted to confirm the efficacy of JZ on SARS-CoV-2 (Fig. 2C and 2D) propagation. The results showed that the average size and plaque number in JZ-treated cells were markedly reduced in a dose-dependent manner. CPE and plaque reduction assays showed that JZ may be a key parameter influencing SARS-CoV-2 activities.

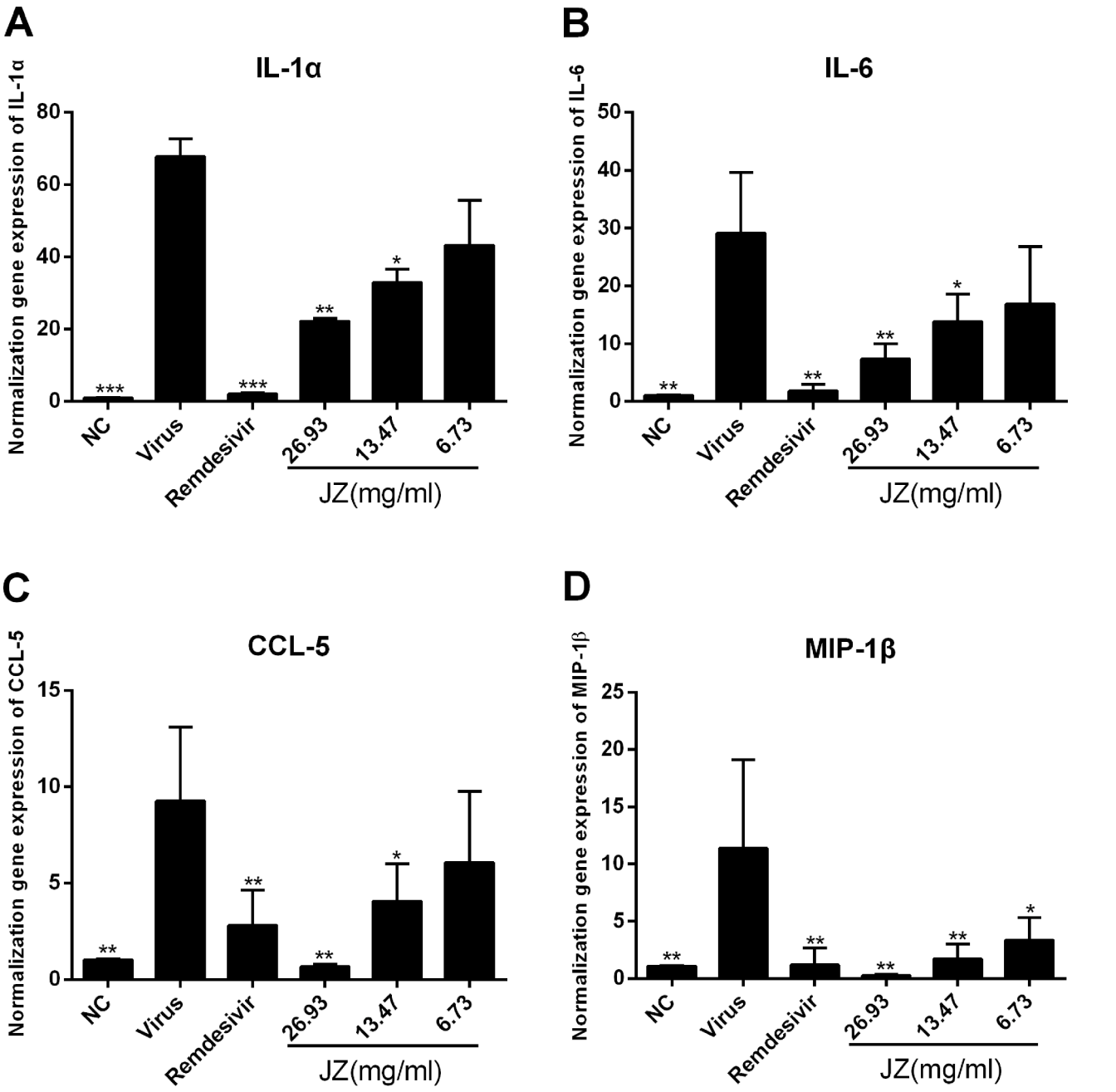

Fig. 4. The mRNA expression levels of IL-1α (A), IL-6 (B), CCL-5 (C) and MIP-1β (D) were detected by RT-qPCR analysis in Vero E6 cells. The values were presented as the means ± S.D. of three individual experiments. * $p < 0.05$; ** $p < 0.01$; *** $p < 0.001$, when compared to the viral control.

The protective effects of JZ against SARS-CoV-2 in mouse model

To estimate the antiviral activity of JZ in mice lethally infected with SARS-CoV-2, the survival of infected mice was determined. After daily observation for 5 days, the survival of mice was shown in Fig. 3. The mortality of the infected mice in the virus group was 60% at 5 days post-infection (d.p.i.). Survival rates of all JZ (896 mg/kg/day, 448 mg/kg/day or 224 mg/kg/day) treated groups were 80%, and were identical to the remdesivir (50 mg/kg/day) treated group (Fig. 3A). The survival time of all JZ (896 mg/kg/day, 448 mg/kg/day or 224 mg/kg/day) and remdesivir groups was 4.80 ± 0.45 d, which was longer than that in the virus group (4.40 ± 0.55 d) ($p < 0.05$). The result suggested that treatment with JZ effectively prolonged survival in mice infected with SARS-CoV-2.

Viral titers reflected the levels of virus needed to initiate infection, and the ability to resist viruses rather than the ability to survive. Thus, the lung virus titers in different groups were determined. The lung virus titers in the JZ (896 mg/kg/day ($p < 0.05$), 448 mg/kg/day ($p < 0.05$) or 224 mg/kg/day ($p < 0.05$)) and remdesivir ($p < 0.01$) groups were markedly decreased compared to those in the virus group (Fig. 3B). The lung virus titer of the virus group was 4.57 ± 0.03, while the virus titers in the lungs treated with JZ (896 mg/kg/day, 448 mg/kg/day or 224 mg/kg/day) or remdesivir were 3.58 ± 0.06, 3.58 ± 0.05, 3.54 ± 0.02 and 1.56 ± 0.03, respectively. These results indicated that JZ inhibited virus titers and virus-induced pneumonia.

Further experiments on the pathological changes in the infected lungs were performed and shown in Fig. 3C. After infection with SARS-CoV-2, the lungs of the uninfected mice showed no changes in histopathology. However, the infected lungs showed hemorrhage, alveolar thickening, and marked infiltration of inflammatory cells. After

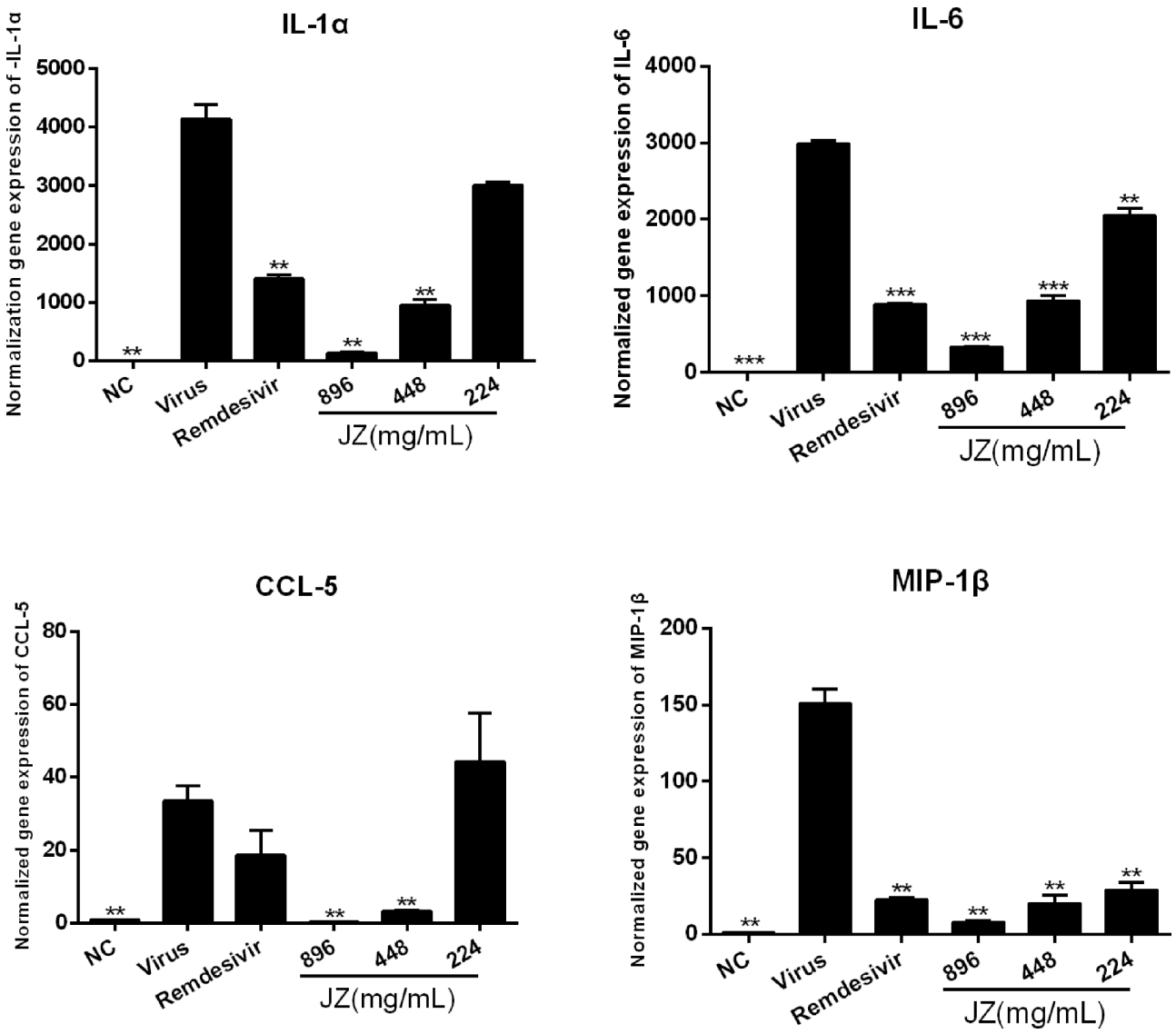

Fig. 5. The inhibitory effects of JZ on viral-induced inflammatory cytokine expression in vivo. The mRNA expression of the IL-1α (A), IL-6 (B), CCL-5 (C) and MIP-1β (D) in the lung of the infected mice were detected by RT-qPCR analysis. The values were presented as the means ± S.D. of three individual experiments. * $p < 0.05$; ** $p < 0.01$; *** $p < 0.001$, when compared to the viral control.

treatment with JZ (896 mg/kg/day, 448 mg/kg/day or 224 mg/kg/day) or remdesivir, the pulmonary function was reduced in a dose dependent manner. These results inferred that JZ could ameliorate lung damage in infected mice.

The inhibitory effects of JZ on viral-induced inflammatory cytokine expression in vitro and in vivo

SARS-CoV-2 infection generally causes inflammatory reactions and cytokine production. Therefore, the mRNA expression levels in vitro and infected mice were detected by RT-qPCR. As shown in Fig. 4, the mRNA expression of IL-1α, IL-6, CCL-5 and MIP-1β in the virus group was markedly up-regulated following SARS-CoV-2 infection ($p < 0.001$ or $p < 0.01$) compared to that in the NC group. Treatment with JZ (26.93 mg/ml and 13.47 mg/ml) notably inhibited this increase in a dose-dependent manner ($p < 0.01$ or $p < 0.05$). The results in SARS-CoV-2 infected mice were similar to those in cells. As shown in Fig. 5, the mRNA expression of IL-1α ($p < 0.01$), IL-6 ($p < 0.001$), CCL-5 ($p < 0.01$) and MIP-1β ($p < 0.01$) was significantly reduced in JZ (896 mg/kg and 448 mg/kg) treated mice compared to virus-infected mice, indicating that JZ may function as an effective anti-inflammatory agent.

The activities of JZ in HCoV-229E infected cells

The cytotoxicity of JZ in Huh-7 cells was evaluated by MTT assay. The TC_{50} value for JZ in Huh-7 cells was 21.19 mg/ml. The IC_{50} value of JZ against HCoV-229E was 5.54 mg/ml, and the selectivity index (SI) of JZ was 3.82. A plaque-reduction assay was also conducted to confirm the efficacy of JZ on HCoV-229E (Fig. 6E and 6F) propagation. The results showed that the average size and plaque number in JZ-treated cells were markedly reduced in a dose-dependent manner. Taken together, the results of the CPE and plaque formation assays indicate that JZ inhibits HCoV-229E proliferation in a dose-dependent manner.

The effects of JZ on the expression of inflammatory cytokines induced by HCoV-229E infection in vitro

To further evaluate the efficacy of JZ against virus-induced inflammation in Huh-7 cells, the mRNA expression levels of inflammatory cytokines, including IL-6, IL-8, TNF-α, MCP-1, MIP-1β and CCL-5, were

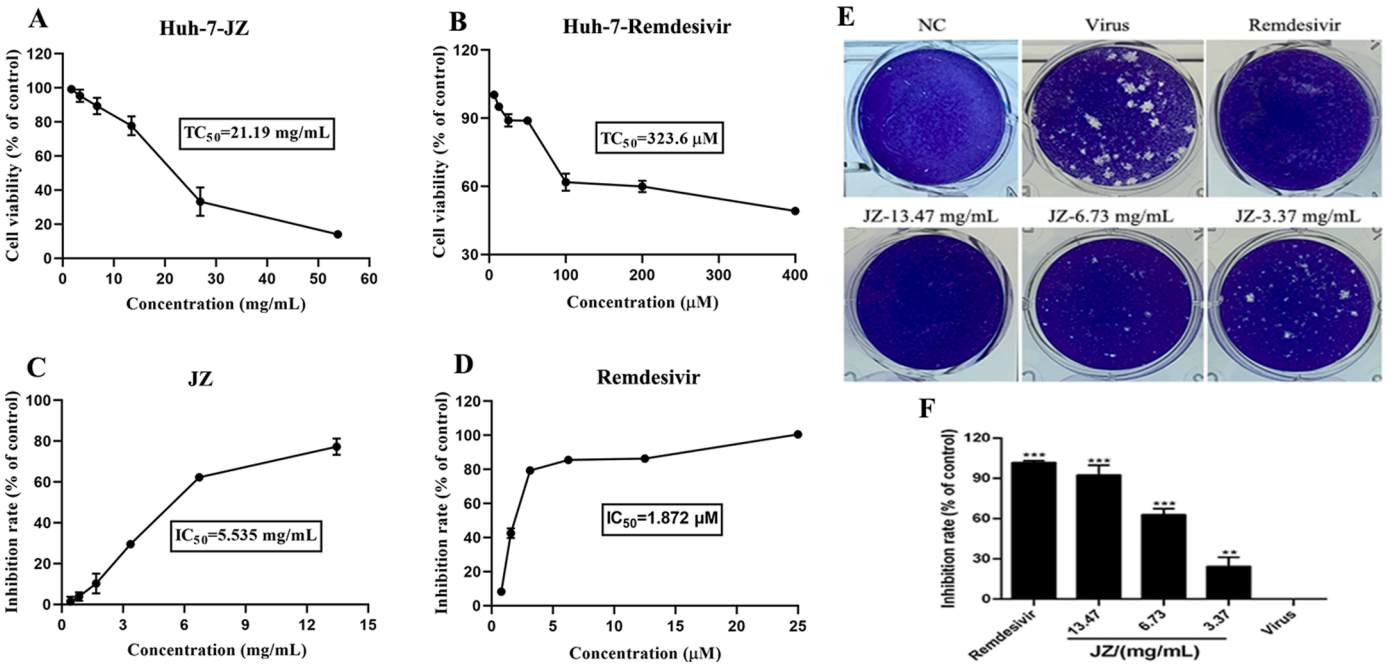

Fig. 6. The activities of JZ in HCoV-229E-infected cells. (A) Cytotoxic effect of JZ in Huh-7 cells was detected by MTT assay; (B) Cytotoxic effect of remdesivir in Huh-7 cells was detected by MTT assay; (C) Inhibitory effect of JZ on HCoV-229E in Huh-7 cells; (D) Inhibitory effect of remdesivir on HCoV-229E in Huh-7 cells; (E) Inhibitory effect of JZ and remdesivir on the plaque formation in Huh-7 cells that induced by HCoV-229E infection; (F) The quantitative analysis of the plaque formation in different groups was analyzed by SPSS ver. 25.0. Data were presented as the mean ± SD obtained from three separate experiments. * $p < 0.05$; ** $p < 0.01$; *** $p < 0.001$, compared with HCoV-229E-infected cells.

tested by RT-qPCR. As shown in Fig. 7, the mRNA expression levels of IL-6 ($p < 0.001$), IL-8 ($p < 0.01$), TNF-α ($p < 0.001$), MCP-1 ($p < 0.01$), MIP-1β ($p < 0.01$) and CCL-5 ($p < 0.05$) in virus group were increased compared to those in the NC group. Moreover, the expression levels of IL-6, IL-8, MCP-1, MIP-1β and CCL-5 were significantly downregulated after JZ treatment (13.47 mg/ml, 6.73 mg/ml and 3.367 mg/ml) in a dose-dependent manner ($p < 0.001$, $p < 0.01$ or $p < 0.05$) and the expression levels of TNF-α was significantly downregulated after JZ treatment (13.47 mg/ml and 6.73 mg/ml) ($p < 0.001$ or $p < 0.01$). These data indicated that inflammatory cytokine expression was effectively suppressed by JZ treatment by regulating host factors.

The effects of JZ on the expression of key proteins associated with the NF-κB/MAPK signaling pathway in vitro

To further characterize the potent anti-inflammatory mechanism of JZ against HCoV-229E, the NF-κB/MAPK signaling pathway was involved, and the protein expression of p-p38 MAPK, p38 MAPK, p-JNK, JNK, p-IκBα, IκBα, p-NF-κB p65 and NF-κB p65 in cells treated with or without JZ was determined (Fig. 8). The results showed that the expression of p-p38 MAPK ($p < 0.001$), p-JNK ($p < 0.01$), p-IκBα ($p < 0.05$) and p-NF-κB p65 ($p < 0.05$) in the virus group was up-regulated compared to that in the NC group, and the expression of IκBα was notably decreased ($p < 0.01$). After JZ treatment, the expression of p-p38 MAPK and p-IκBα was markedly suppressed ($p < 0.01$) by JZ (13.47 mg/ml and 6.73 mg/ml), and the expression of p-NF-κB p65 was markedly suppressed by all the three doses of JZ (13.47 mg/ml ($p < 0.001$), 6.73 mg/ml ($p < 0.01$) and 3.37 mg/ml ($p < 0.01$)). Moreover, the expression of IκBα was up-regulated at a concentration of 13.47 mg/ml ($p < 0.05$), and the expression of p-JNK was reduced at the concentrations of 13.47 mg/ml ($p < 0.05$) and 6.73 mg/ml ($p < 0.05$) compared to the virus group.

Decrease in apoptosis with JZ induced by HCoV-229E infection in Huh-7 cells

The apoptosis induction rate indicates the efficacy of JZ treatment to a certain extent. An Annexin V-FITC apoptosis detection kit was used to further study the anti-apoptotic effect of JZ (Fig. 9A). Virus-induced apoptosis of Huh-7 cells was markedly elevated 48 h post-infection ($p < 0.001$) compared to the NC group. Notably, JZ treatment (6.73 mg/ml and 3.37 mg/ml) effectively suppressed the percentage of apoptotic cells relative to the virus group in a dose-dependent manner ($p < 0.01$).

After treatment with various concentrations of JZ, Huh-7 cells infected with HCoV-229E were stained with JC-1. JC-1 presents red florescence under florescent electron microscopy by aggregating in normal mitochondria, Huh-7 cells infected by HCoV-229E resulted in dissipation of ΔΨm, which was visualized as increased green florescence by JC-1 staining. As shown in Fig. 9B, the increased green florescence in the virus-infected group was decreased by JZ, while remdesivir treatment exerted little or a weak effect.

The intrinsic pathways that activate apoptosis were induced by caspase 9 activation. Mature caspase 9 further motivates effector caspase 3, which cleaves PARP (poly (ADP-ribose) polymerase) and terminates DNA repair. We determined the processing of procaspase 9 and procaspase 3 by western blotting analysis. As shown in Fig. 9C and D, the cleavage of procaspase 9 caused the processing of procaspase 3 and activation of caspase 3 in the virus group, the expression of caspase 9, 3 and PARP in the virus group were significantly decreased ($p < 0.001$) compared to that in the NC group. Notably, JZ (13.47 mg/ml, 6.73 mg/ml and 3.37 mg/ml) and remdesivir treatment exerted significant anti-apoptotic effects by decreasing ($p < 0.001$) the expression of cleaved caspase 3 and p-PARP in virus-infected cells, and the expression of cleaved caspase 9 was also reduced ($p < 0.001$) after JZ treatment (13.47 mg/ml and 6.73 mg/ml). Moreover, the expression of caspase 9 was markedly up-regulated when treatment with JZ (13.47 mg/ml and 6.73 mg/ml) ($p < 0.001$), and the expression of caspase 3 was markedly up-regulated when treatment with JZ (13.47 mg/ml ($p < 0.001$) and

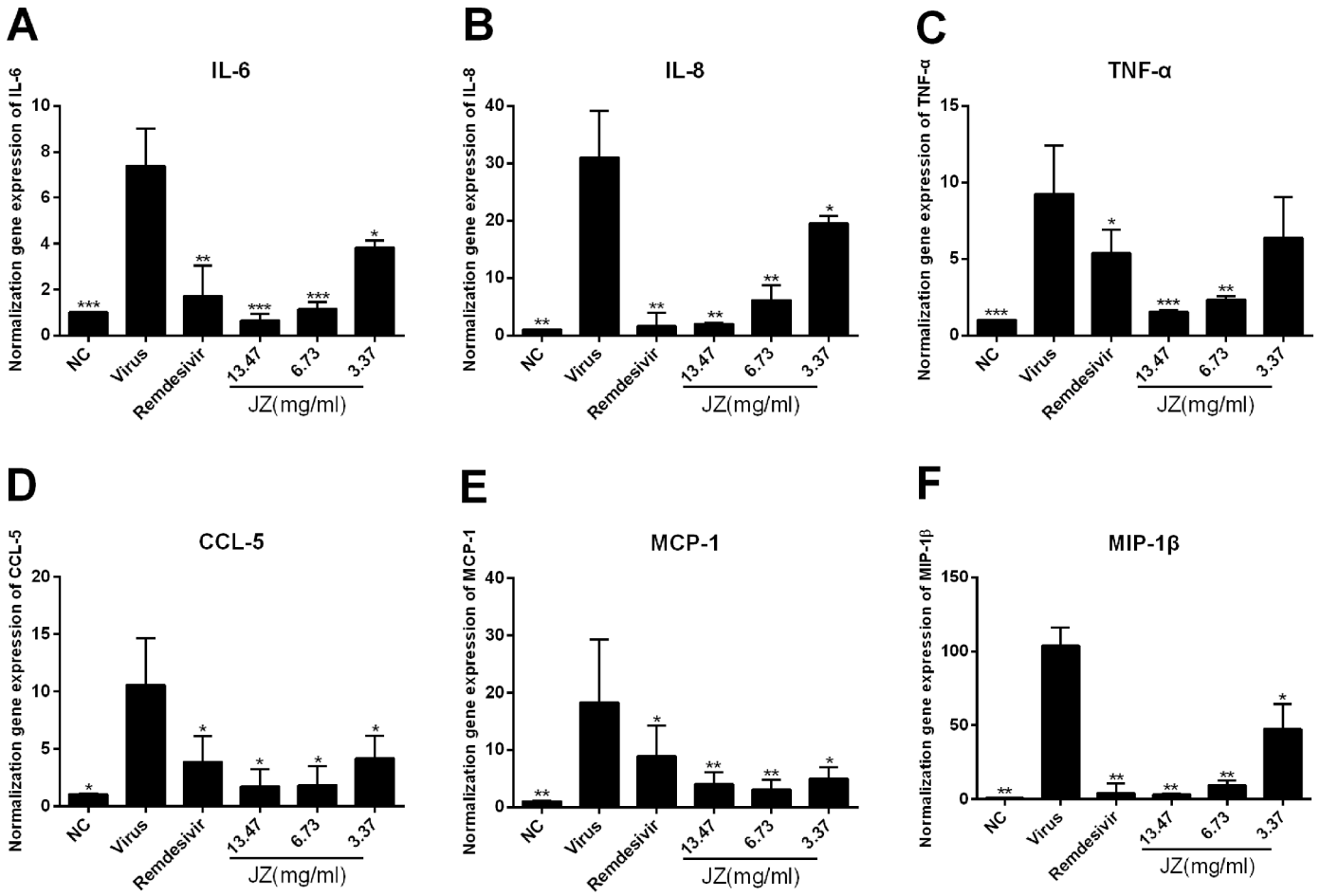

Fig. 7. The effects of JZ on the expression of inflammatory cytokines induced by HCoV-229E infection *in vitro*. (A-F) The mRNA expression of IL-6 (A), IL-8 (B), TNF-α (C), CCL2/MCP-1 (D), CCL4/MIP-1β (E) and CCL-5 (F) in Huh-7 cells infected by HCoV-229E were detected by RT-qPCR analysis. Data were presented as the mean ± SD obtained from three separate experiments. * $p < 0.05$; ** $p < 0.01$; *** $p < 0.001$, compared with HCoV-229E-infected cells.

6.73 mg/ml ($p < 0.05$)), while the expression of PARP was notably up-regulated in the JZ treatment group at a concentration of 13.47 mg/ml ($p < 0.01$). Altogether, these results suggested that JZ effectively inhibited the apoptosis induced by HCoV-229E infection in Huh-7 cells.

Discussion

Coronavirus has already caused three outbreaks in the past two decades: SARS, MERS and present COVID-19. This pandemic caused by SARS-CoV-2 poses a huge menace to human public health and has caused enormous economic losses and psychosocial impacts on a global scale. Due to the limitations of COVID-19 vaccines, there exists an urgent need for effective and safe antivirals. Notably, some TCM have become an acceptable therapy and many TCM prescriptions exhibit unique effects on virus infection especially regulating the immune functions of host organisms. These mechanisms make some TCM prescriptions effective antivirals, especially for combating COVID-19 in China. JZ is a frontline pediatric medicine in China for treating diseases caused by some viral infections and shows marked efficacy. However, little is known about the antiviral effect of JZ against SARS-CoV-2 and HCoV-229E. Herein, the purpose of this study was to reveal the antiviral mechanisms of JZ on SARS-CoV-2 and HCoV-229E.

The CPE inhibition assay and plaque formation assay remain the gold standard for quantifying the infectious virions and antivirals directly. Thus, we conducted CPE inhibition assay and plaque formation assay to demonstrate the antiviral effects of JZ against SARS-CoV-2 infection in vitro. We demonstrated that JZ protected cells from virus-induced cell death with an IC_{50} of 3.999 mg/ml and that the SI index of JZ was 19.0. Meanwhile, plaque formation was suppressed by JZ treatment in SARS-CoV-2 infected cells. To reveal the deeper effectiveness of JZ against other coronaviruses, we further determined the antiviral effect of JZ on HCoV-229E. The results also showed that JZ effectively reduced CPE and plaque formation induced by HCoV-229E infection. The results indicated that JZ could influence SARS-CoV-2 and HCoV-229E activities.

Infected animal models play a vital role in investigating COVID-19 pathogenesis, and evaluating novel therapies and vaccines. The previously reported hACE2 transgenic mice model and Ad5-hACE2-transduced mice model both exhibited weight loss after infection with SARS-CoV-2, but one had no deaths reported, and the other was non-lethal (Bao et al., 2020; Sun et al., 2020). Accordingly, we established a lethal hACE2 transgenic mice model of SARS-CoV-2 based on the performance of other mouse models. Subsequently, we performed animal experiments on SARS-CoV-2 infected hACE2 transgenic mice to further investigate the dose-dependent effects of JZ treatment on survival and virus titer in vivo. In our lethal SARS-CoV-2 infection mouse model, oral dosing with wide range concentrations of JZ effectively prevented signs of virus infection. The results showed that JZ treatment significantly reduced the mortality of virus-infected mice and prolonged the mice survival rate. Furthermore, oral administration of JZ reduced virus titers in virus-infected mice to a certain extent, which might lead to an inhibition of early-response proinflammatory cytokines and was associated with lower chemokine levels. In this study, there were no significant toxicity problems.

SARS-CoV-2 infection is generally accompanied by invasive

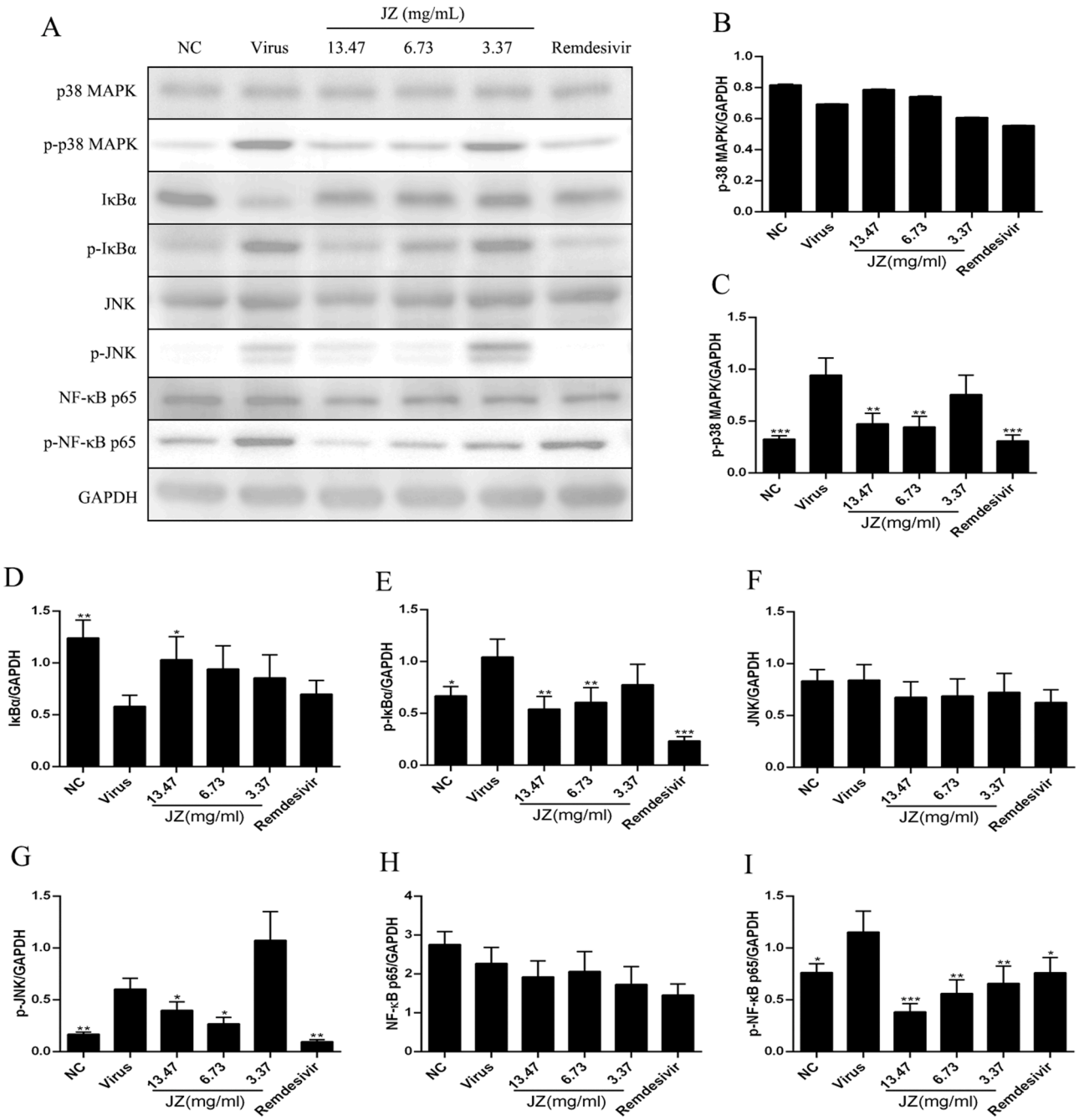

Fig. 8. The effects of JZ on the expression of key proteins associated with the NF-κB/MAPK signaling pathway *in vitro*. (A) The protein expressions of p-p38 MAPK, p38 MAPK, p-JNK, JNK, p-IκBα, IκBα, p-NF-κB p65 and NF-κB p65 in Huh-7 cells was detected by western blot analysis; (B-I) The quantitative analysis of the p-p38 MAPK, p38 MAPK, p-JNK, JNK, p-IκBα, IκBα, p-NF-κB p65 and NF-κB p65 proteins was analyzed by Image J. Data were presented as the means ± SD of three individual experiments. * $p < 0.05$; ** $p < 0.01$; *** $p < 0.001$, when compared to the viral control.

inflammatory response followed by the release of a large amount of pro-inflammatory cytokines, and this event is known as a cytokine storm. Several cytokine profile analysis studies of COVID-19 patients indicate that cytokine storms are directly associated with lung injury, multiple organ failure and undesirable prognosis (Chen et al., 2020a), suggesting that correlated cytokine levels could be used to evaluate the outcome and prognosis of COVID-19 (Wan et al., 2020). Different cytokines contribute to cytokine storms in COVID-19 patients, including CCL-2/MCP-1, CCL-4/MIP-1β, CCL-5, CXCL-10/IP-10, IFN-γ, TNF-α, and IL-6 (Nile et al., 2020). Accordingly, in this study, the IL-1α, IL-6, CCL-5 and CCL-4/MIP-1β levels in Vero E6 cells infected with SARS-CoV-2 were markedly elevated, and suppressed by JZ in a dose-dependent manner. Additionally, the potential effect of JZ on inhibiting cytokine storms induced by SARS-CoV-2 infection was investigated in a lethal hACE2 transgenic mouse model. The results showed that JZ treatment similarly mitigated the increases in IL-1α, IL-6, CCL-5 and CCL-4/MIP-1β in a dose-dependent manner. Moreover, the potential effect of JZ on inhibiting cytokine storms induced by HCoV-229E infection was further investigated in Huh-7 cells, and the increased expression levels of IL-6, IL-8, TNF-α, CCL2/MCP-1, CCL4/MIP-1β and CCL-5 were also markedly suppressed by JZ.

Severe SARS accompanied by elevated cytokines reflects a dysregulation of the immune response. NF-κB activation is a marker of most viral infections (including CoVs) and results in immune and pathogenic

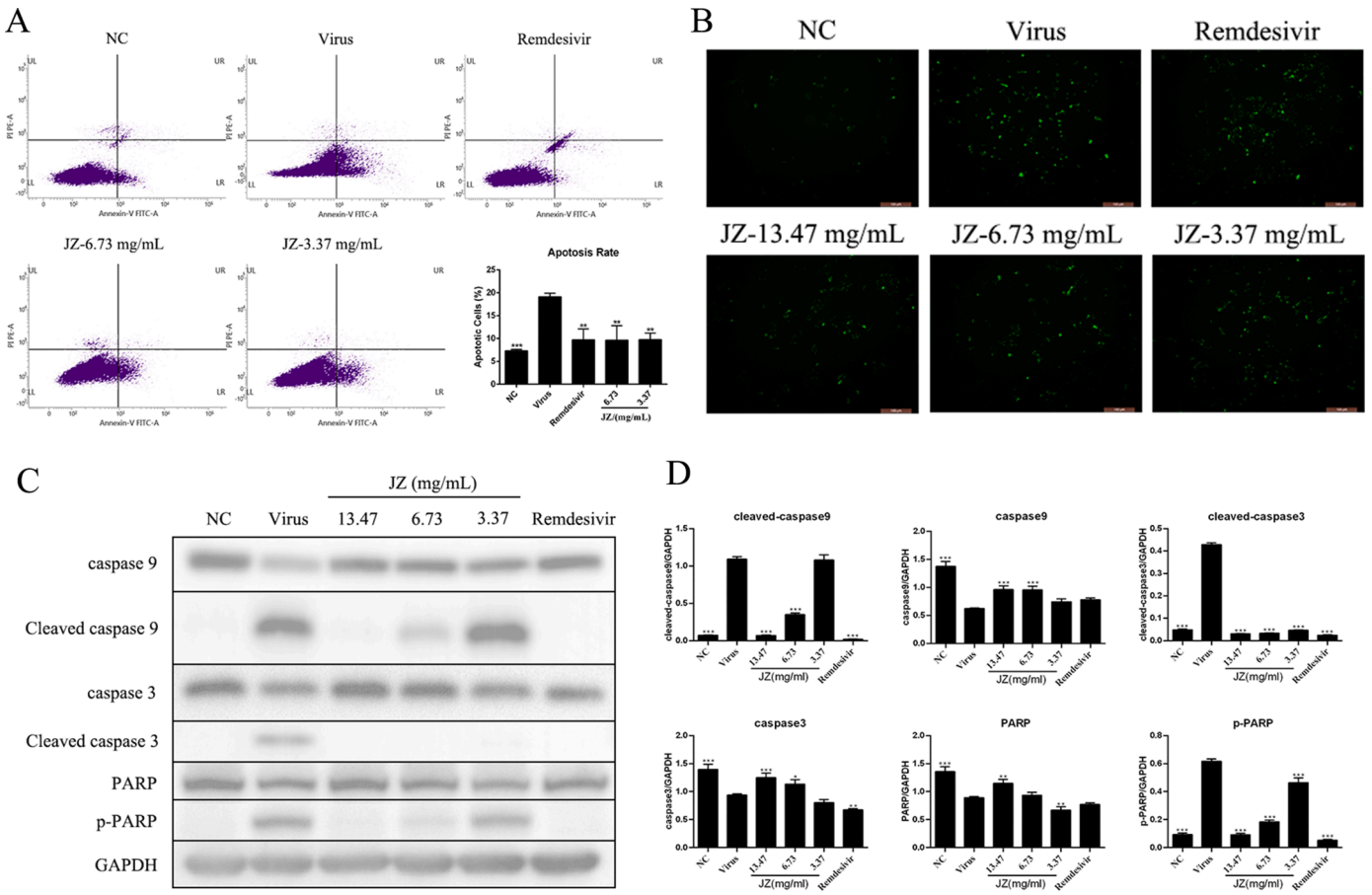

Fig. 9. Decrease in apoptosis with JZ induced by HCoV-229E infection in Huh-7 cells. (A) Percentage of apoptotic cells in Huh-7 cells were detected by flow cytometry and was analyzed by SPSS ver. 25.0; (B) Huh-7 cells were stained by JC-1 and the change of ΔΨm was detected by fluorescence microscopy; (C) The protein expressions of caspase 9, caspase 3, Cleaved caspase 9, Cleaved caspase 3, PARP and p-PARP in Huh-7 cells were detected by western blot analysis; (D) The quantitative analysis of the caspase 9, Cleaved caspase 9, caspase 3, Cleaved caspase 3, PARP and p-PARP proteins was analyzed by Image J. The values were presented as the means ± SD of three individual experiments. * $p < 0.05$; ** $p < 0.01$; *** $p < 0.001$, when compared to the viral control.

responses (Smits et al., 2010). Accordingly, NF-κB has become a promising therapeutic target against infectious diseases, and more than 700 NF-κB inhibitors have been described (Gilmore and Herscovitch, 2006). Subsequently, we aimed to reveal the molecular mechanism of LS against coronavirus infection. Western blotting was performed to evaluate the regulatory effect of JZ on the NF-κB/MAPK signaling pathway, which contributes to inflammatory alleviation. The results showed that the NF-κB/MAPK signaling pathway was activated by HCoV-229E infection in Huh-7 cells and that the expression of IκBα was increased as previously described (Schmitz et al., 2014). Notably, JZ decreased the activation of p-p38 MAPK, p-JNK, p-NF-κB p65 and p-IκBα induced by HCoV-229E infection, while increasing IκBα expression. These findings suggested that the inhibition of the activation of the NF-κB/MAPK signaling pathway seemed to be the underlying mechanism by which JZ alleviated CoVs-induced inflammation. The cytokine profile regulation indicated that JZ might exhibit inhibitory effect on cytokine storms induced by coronavirus.

It has been reported that many viruses and their viral proteins are able to induce replication-dependent apoptosis (Kvansakul, 2017), including SARS-CoV-2 and HCoV-229E, and so on. It has been demonstrated that SARS-CoV-2 is associated with activation of caspase 8 that trigger cell apoptosis and inflammatory cytokine (Li et al., 2020), and HCoV-229E infection induce the upregulation of genes of apoptosis result in cell death (Rezaie et al., 2020). Furthermore, apoptosis and P53 signaling pathway activation in lymphocytes induced by SARS-CoV-2 infection may be the cause of lymphopenia in COVID-19 patient (Xiong et al., 2020). Notably, the apoptosis induced by human coronavirus infection has been widely investigated, making us assume that apoptosis may play a crucial role in the pathogenesis of human coronaviruses (Fung and Liu, 2019). Apoptosis is generally associated with the activation of a family of caspases. Stimuli such as virus infection convert death signals into mitochondria resulting in mitochondrial injury and the release of cytochrome c (cytC) into the cytoplasm. cytC forms an apoptosome complex with apaf-1 in the presence of dATP and subsequently recruits procaspase 9 to activate it. Activation of caspase 9 indicates activation of mitochondria-mediated apoptotic pathways. The initiator of caspase 9 processes self-cleavage and activation after receiving apoptotic signals. These up-stream caspases subsequently activate effector caspases 3, 6, and 7, and caspase 3 is the most representative. Caspase 3 cleaves PARP and activates endonuclease leading to DNA repair termination and finally to cell apoptosis (Saleh et al., 1999). The decreased apoptosis induction rate might be associated with the efficacy of JZ. Thus, we further investigated the anti-apoptotic effect of JZ on HCoV-229E infected cells. JZ effectively prevented mitochondrial injury and reduced the percentage of apoptotic Huh-7 cells induced by HCoV-229E infection. Furthermore, JZ suppressed the activation of caspase-9and caspase-3 and reduced the increased expression of cleaved caspase-9, caspase-3 and p-PARP caused by HCoV-229E infection. These findings further proved the efficacy of JZ against coronavirus.

Conclusions

In conclusion, our findings indicated that JZ, which consists of gallic acid 1.97 mg/g, baicalin 20.69 mg/g, glycyrrhizic acid 4.92 mg/g,

hyodeoxycholic acid 4.86 mg/g, cholic acid 4.07 mg/g, could protect against cell death from SARS-CoV-2 and HCoV-229E infection and suppress the plaque formation in vitro. In our lethal SARS-CoV-2 infection mouse model, JZ (896 mg/kg/day, 448 mg/kg/day or 224 mg/kg/day) improved the survival of SARS-CoV-2 infected mice, alleviated lung inflammation and reduced lung virus titers. In further studies, JZ inhibited the pro-inflammatory cytokines induced by SARS-CoV-2 infection and similarly inhibited the inflammatory response by regulating the NF-κB/MAPK signaling pathway in Huh-7 cells infected with HCoV-229E. Of note, our study demonstrated that JZ suppressed the activation of mitochondria-mediated apoptotic pathways and prevented cells from undergoing apoptosis induced by HCoV-229E infection. Consequently, these findings are conducive to the application of JZ in the clinical treatment of COVID-19 in combination with existing therapies.

Declaration of Competing Interest

All the authors declare that the research was conducted in the absence of any commercial or financial relationships that could be construed as a potential conflict of interest.

Acknowledgments

This work was supported by National Key R&D Program of China (2020YFA0708002), National Natural Science Foundation of China (82004033), Basic and Applied Basic Research Foundation of Guangdong Province (2020A1515111155), Emergency Key Program of Guangzhou Laboratory (EKPG21–06), Macao Science and Technology Development Fund (0172/2019/A3, 0042/2020/A, 0022/2021/A1), Guangdong Provincial Department of Natural Resources project (GDNRC[2021]51), Innovation project of Foshan Science and Technology Bureau (2020001000206), Guangzhou Science and Technology Bureau key research and development projects (20200804001), Novel Coronavirus Prevention and control Project of Guangdong Province science and Technology Department and Novel Coronavirus Prevention and Control Project of Guangdong Province (2020B111110001, 2020B1111300005, 2020B111112002), Department of Education of Guangdong Provincial (2020KZDZX1159), Science Research Project of the Guangdong Province (Nos. 2020B111110001), Guangzhou key laboratory for clinical rapid diagnosis and early warning of infectious diseases (202102100003).

References

Bao, L., Deng, W., Huang, B., Gao, H., Liu, J., Ren, L., Wei, Q., Yu, P., Xu, Y., Qi, F., Qu, Y., Li, F., Lv, Q., Wang, W., Xue, J., Gong, S., Liu, M., Wang, G., Wang, S., Song, Z., Zhao, L., Liu, P., Zhao, L., Ye, F., Wang, H., Zhou, W., Zhu, N., Zhen, W., Yu, H., Zhang, X., Guo, L., Chen, L., Wang, C., Wang, Y., Wang, X., Xiao, Y., Sun, Q., Liu, H., Zhu, F., Ma, C., Yan, L., Yang, M., Han, J., Xu, W., Tan, W., Peng, X., Jin, Q., Wu, G., Qin, C., 2020. The pathogenicity of SARS-CoV-2 in hACE2 transgenic mice. Nature 583, 830–833.

Cavic, M., Krivokuca, A., Boljevic, I., Spasic, J., Mihajlovic, M., Pavlovic, M., Damjanovic, A., Radosavljevic, D., Jankovic, R., 2021. Exploring the real-world effect of the SARS-CoV-2 pandemic on the molecular diagnostics for cancer patients and high-risk individuals. Expert Rev. Mol. Diagn. 21, 101–107.

Chen, G., Wu, D., Guo, W., Cao, Y., Huang, D., Wang, H., Wang, T., Zhang, X., Chen, H., Yu, H., Zhang, X., Zhang, M., Wu, S., Song, J., Chen, T., Han, M., Li, S., Luo, X., Zhao, J., Ning, Q., 2020a. Clinical and immunological features of severe and moderate coronavirus disease 2019. J. Clin. Invest. 130, 2620–2629.

Chen, N., Zhou, M., Dong, X., Qu, J., Gong, F., Han, Y., Qiu, Y., Wang, J., Liu, Y., Wei, Y., Xia, J., Yu, T., Zhang, X., Zhang, L., 2020b. Epidemiological and clinical characteristics of 99 cases of 2019 novel coronavirus pneumonia in Wuhan, China: a descriptive study. Lancet 395, 507–513.

Fehr, A.R., Perlman, S., 2015. Coronaviruses: an overview of their replication and pathogenesis. Methods Mol. Biol. 1282, 1–23.

Fung, T.S., Liu, D.X., 2019. Human Coronavirus: host-pathogen interaction. Annu. Rev. Microbiol. 73, 529–557.

Gilmore, T.D., Herscovitch, M., 2006. Inhibitors of NF-kappaB signaling: 785 and counting. Oncogene 25, 6887–6899.

Gorse, G.J., O'Connor, T.Z., Hall, S.L., Vitale, J.N., Nichol, K.L., 2009. Human coronavirus and acute respiratory illness in older adults with chronic obstructive pulmonary disease. J. Infect. Dis. 199, 847–857.

Hou, A., Liu, Y., Xin, D., Zhao, Y., 2009. Therapeutic effect of Jinzhen oral liquid inhibiting respiratory syncytial virus, SARS virus and mycoplasma pneumoniae. Chin. J. PMP 16, 1454–1455.

Huang, C., Wang, Y., Li, X., Ren, L., Zhao, J., Hu, Y., Zhang, L., Fan, G., Xu, J., Gu, X., Cheng, Z., Yu, T., Xia, J., Wei, Y., Wu, W., Xie, X., Yin, W., Li, H., Liu, M., Xiao, Y., Gao, H., Guo, L., Xie, J., Wang, G., Jiang, R., Gao, Z., Jin, Q., Wang, J., Cao, B., 2020. Clinical features of patients infected with 2019 novel coronavirus in Wuhan, China. Lancet 395, 497–506.

Jan, J., Cheng, T., Juang, Y., Ma, H., Wu, Y., Yang, W., Cheng, C., Chen, X., Chou, T., Shie, J., Cheng, W., Chein, R., Mao, S., Liang, P., Ma, C., Hung, S., Wong, C., 2021. Identification of existing pharmaceuticals and herbal medicines as inhibitors of SARS-CoV-2 infection. PNAS 118, e2021579118.

Kvansakul, M., 2017. Viral infection and apoptosis. Viruses 9.

Li, S., Zhang, Y., Guan, Z., Li, H., Ye, M., Chen, X., Shen, J., Zhou, Y., Shi, Z.L., Zhou, P., Peng, K., 2020. SARS-CoV-2 triggers inflammatory responses and cell death through caspase-8 activation. Signal Transduct. Target Ther. 5 (1), 235.

Liu, J., Zhang, G.L., Huang, G.Q., Li, L., Li, C.P., Wang, M., Liang, X.Y., Xie, D., Yang, C. M., Li, Y., Sun, X.R., Zhang, H.S., Wan, B.S., Zhang, W.H., Yu, H., Zhang, R.Y., Yu, Y. N., Wang, Z., Wang, Y.Y., 2014. Therapeutic effect of Jinzhen oral liquid for hand foot and mouth disease: a randomized, multi-center, double-blind, placebo-controlled trial. PLoS ONE 9, e94466.

Lu, H., 2020. Drug treatment options for the 2019-new coronavirus (2019-nCoV). Biosci. Trends 14, 69–71.

Ma, Q., Huang, W., Zhao, J., Yang, Z., 2020. Liu Shen Wan inhibits influenza a virus and excessive virus-induced inflammatory response via suppression of TLR4/NF-kappaB signaling pathway in vitro and in vivo. J. Ethnopharmacol. 252, 112584.

Nile, S.H., Kai, G., 2020. Recent clinical trials on natural products and traditional chinese medicine combating the COVID-19. Indian J. Microbiol. 1–6.

Nile, S.H., Nile, A., Qiu, J., Li, L., Jia, X., Kai, G., 2020. COVID-19: pathogenesis, cytokine storm and therapeutic potential of interferons. Cytokine Growth Factor Rev. 53, 66–70.

Park, K.I., Park, H.S., Kang, S.R., Nagappan, A., Lee, D.H., Kim, J.A., Han, D.Y., Kim, G.S., 2011. Korean Scutellaria baicalensis water extract inhibits cell cycle G1/S transition by suppressing cyclin D1 expression and matrix-metalloproteinase-2 activity in human lung cancer cells. J. Ethnopharmacol. 133, 634–641.

Pfaffl, M.W., 2001. A new mathematical model for relative quantification in real-time RT-PCR. Nucleic. Acids Res. 29, e45.

Rezaie, A., Leite, G.G.S., Melmed, G.Y., Mathur, R., Villanueva-Millan, M.J., Parodi, G., Sin, J., Germano, J.F., Morales, W., Weitsman, S., Kim, S.Y., Park, J.H., Sakhaie, S., Pimentel, M., 2020. Ultraviolet A light effectively reduces bacteria and viruses including coronavirus. PLoS ONE 15 (7), e0236199.

Reed, L.J., Muench, H., 1938. A simple method of estimating fifty per cent endpoints12. Am. J. Epidemiol. 27, 493–497.

Saleh, A., Srinivasula, S.M., Acharya, S., Fishel, R., Alnemri, E.S., 1999. Cytochrome c and dATP-mediated oligomerization of Apaf-1 is a prerequisite for procaspase-9 activation. J. Biol. Chem. 274, 17941–17945.

Schmitz, M.L., Kracht, M., Saul, V.V., 2014. The intricate interplay between RNA viruses and NF-kappaB. Biochim. Biophys. Acta 1843, 2754–2764.

Smits, S.L., de Lang, A., van den Brand, J.M., Leijten, L.M., van, I.W.F., Eijkemans, M.J., van Amerongen, G., Kuiken, T., Andeweg, A.C., Osterhaus, A.D., Haagmans, B.L., 2010. Exacerbated innate host response to SARS-CoV in aged non-human primates. PLoS Pathog. 6, e1000756.

Su, S., Wong, G., Shi, W., Liu, J., Lai, A.C.K., Zhou, J., Liu, W., Bi, Y., Gao, G.F., 2016. Epidemiology, genetic recombination, and pathogenesis of coronaviruses. Trends Microbiol. 24, 490–502.

Jr. Sun, J., Zhuang, Z., Zheng, J., Li, K., Wong, R.L., Liu, D., Huang, J., He, J., Zhu, A., Zhao, J., Li, X., Xi, Y., Chen, R., Alshukairi, A.N., Chen, Z., Zhang, Z., Chen, C., Huang, X., Li, F., Lai, X., Chen, D., Wen, L., Zhuo, J., Zhang, Y., Wang, Y., Huang, S., Dai, J., Shi, Y., Zheng, K., Leidinger, M.R., Chen, J., Li, Y., Zhong, N., Meyerholz, D. K., McCray, P.B., Perlman, S., Zhao, J., 2020. Generation of a broadly useful model for COVID-19 pathogenesis, vaccination, and treatment Cell 182, 734–743. e735.

Wan, S., Yi, Q., Fan, S., Lv, J., Zhang, X., Guo, L., Lang, C., Xiao, Q., Xiao, K., Yi, Z., Qiang, M., Xiang, J., Zhang, B., Chen, Y., 2020. Characteristics of lymphocyte subsets and cytokines in peripheral blood of 123 hospitalized patients with 2019 novel coronavirus pneumonia (NCP). medRxiv, 2020.2002.2010.20021832.

Wang, C., Horby, P.W., Hayden, F.G., Gao, G.F., 2020. A novel coronavirus outbreak of global health concern. Lancet 395, 470–473.

Wang, C., Wang, Z., Wang, G., Lau, J.Y., Zhang, K., Li, W., 2021a. COVID-19 in early 2021: current status and looking forward. Signal Transduct. Target Ther. 6, 114.

Wang, W.Y., Xie, Y., Zhou, H., Liu, L., 2021b. Contribution of traditional Chinese medicine to the treatment of COVID-19. Phytomedicine 85, 153279.

WHO, 2020. Coronavirus disease (COVID-19) outbreak. https://www.who.int/(assessed June 24, 2021).

Xiong, Y., Liu, Y., Cao, L., Wang, D., Guo, M., Jiang, A., Guo, D., Hu, W., Yang, J., Tang, Z., Wu, H., Lin, Y., Zhang, M., Zhang, Q., Shi, M., Liu, Y., Zhou, Y., Lan, K., Chen, Y., 2020. Transcriptomic characteristics of bronchoalveolar lavage fluid and peripheral blood mononuclear cells in COVID-19 patients. Emerg. Microbes. Infect. 9, 761–770.

Zhang, M., He, Z., Wen, L., Wu, J., Yuan, L., Lu, Y., Guo, C., Zhu, L., Deng, S., Yuan, H., 2010. Cadmium suppresses the proliferation of piglet Sertoli cells and causes their

DNA damage, cell apoptosis and aberrant ultrastructure. Reprod. Biol. Endocrinol. 8, 97.
Zhu, N., Zhang, D., Wang, W., Li, X., Yang, B., Song, J., Zhao, X., Huang, B., Shi, W., Lu, R., Niu, P., Zhan, F., Ma, X., Wang, D., Xu, W., Wu, G., Gao, G.F., Tan, W., 2019. China Novel Coronavirus, I., Research, T., 2020. A novel coronavirus from patients with pneumonia in China. N. Engl. J. Med. 382, 727–733.
Zong, S., Sun, L., Lyu, Y., Zhou, J., Wang, Z., Xiao, W., 2018. Effect of Jinzhen oral liquid on NF-κB, MAPK signaling pathway in mice with LPS-induced acute lung I. Chin. J ETMF 24, 155–159.